

LASER DOPPLER VELOCIMETRY UNCERTAINTY ANALYSIS FOR ROTOR BLADE TIP VORTEX MEASUREMENTS

Preston B. Martin,* Gregory J. Pugliese* and J. Gordon Leishman†

*Department of Aerospace Engineering,
University of Maryland,
College Park, Maryland 20742, USA*

Laser Doppler velocimetry (LDV) measurements were made in the wake of a sub-scale helicopter rotor operating in hover. The measurements were part of a systematic study of the effect of tip planform on the structure and evolution of the rotor wake vortex system. A procedure for three-dimensional LDV alignment using a laser beam profiler was developed. A method for detailed uncertainty analysis of the beam alignment and vortex measurement technique is described. Sources of uncertainty are identified with optics calibration, data acquisition, and data reduction. Precision and bias limits are estimated using velocity profile measurements across a representative vortex core. Sources of LDV bias are discussed. Experimental and theoretical results were used to better understand LDV gradient bias in vortical flows. Spatial resolution requirements were also established for detailed velocity field profiling of rotor blade tip vortices.

Nomenclature

<p>A = LDV transformation matrix defined by the optical geometric configuration</p> <p>B = source bias limit</p> <p>B_i = elemental source of bias uncertainty</p> <p>C_T = rotor thrust coefficient, $T/\rho\pi\Omega^2R^4$</p> <p>c = rotor blade chord</p> <p>d_f = fringe spacing in the LDV probe volume</p> <p>d_p = seed particle geometric diameter</p> <p>D_m = width of LDV probe volume</p> <p>f = Doppler frequency on a single channel</p> <p>F = vector of the Doppler frequency on each channel</p> <p>L_m = length of LDV probe volume, or size of hotwire</p> <p>m = slope of beam with respect to the hub y-axis</p> <p>N = sample size (number of measurements)</p> <p>P = source precision limit</p> <p>P_i = elemental source of precision uncertainty</p> <p>R = rotor blade radius</p> <p>r = radial position from vortex core</p> <p>r_c = vortex viscous core radius defined as half the distance between velocity peaks</p> <p>\bar{r} = r/r_c</p> <p>res = instrument resolution (dimensional)</p> <p>s = shift frequency of a single channel</p> <p>t_v = student t-factor</p> <p>T = rotor thrust</p> <p>V = velocity vector of flow (u, v, w) defined along the traverse coordinates (x, y, z)</p> <p>V_c = convection velocity of vortex core</p>	<p>V_θ = vortex tangential (swirl) velocity or phase resolved velocity</p> <p>\bar{V}_θ = phase averaged velocity</p> <p>V'_θ = vortex tangential (swirl) velocity</p> <p>x, y, z = traverse position in hub frame of reference</p> <p>u, v, w = velocity components measured in hub frame</p> <p>u' = x-component of phase resolved velocity</p> <p>\bar{u} = x-component of phase averaged velocity</p> <p>U_o = general reference velocity</p> <p>Z_R = Raleigh length of laser beam</p> <p>α = ratio of probe length to vortex core radius</p> <p>δ = uncertainty in a variable</p> <p>Δx = beam profiler measurement of distance between centroids of intensity distribution</p> <p>Δy = traverse movement along y-axis of hub frame</p> <p>κ = half angle of beam crossing</p> <p>λ = laser beam wavelength</p> <p>ν = measured burst frequency of scattered light from a single channel : $\nu = f + s$</p> <p>θ = transmitting angle of fiber optic probe with respect to the hub y-axis</p> <p>ρ = fluid density</p> <p>ρ_p = seed particle density</p> <p>σ = standard deviation of measurement</p> <p>σ_e = rotor thrust weighted solidity</p> <p>τ = burst transit time</p> <p>Ω = angular velocity of rotor blade</p> <p>ψ = blade azimuth measured in the y-z plane</p>
---	---

*Graduate Research Assistant, Member

†Associate Professor, Senior Member

Copyright © 2000 by P. B. Martin, G. J. Pugliese and J. G. Leishman. Published by the American Institute of Aeronautics and Astronautics, Inc. with permission.

Introduction

An improved understanding of the formation and evolution of the vortices trailed from a helicopter rotor blade is key to advanced vehicle designs. Measurements providing insight into vortex formation near the blade tip aid the development of advanced design strategies to alleviate vortex induced rotor phenomena, including induced airloads, vibrations, and acoustics. Detailed measurement uncertainty analysis is critical to this process, especially when results are used for computational method validation or are compared between various facilities. Empirically validated rotor blade wake models are becoming more integrated into comprehensive rotor codes. As a result, measurement uncertainty propagates directly into the performance uncertainty of the helicopter.

Rotor wake flow physics in both hovering and forward flight have been measured over the past three decades using a variety of techniques including LDV¹⁻¹² and hotwires.¹³⁻¹⁷ Measurement uncertainty estimates often go unreported or are sometimes given in terms of a single number. The sources of uncertainty are coupled to both the critical flow features (such as a vortex core) and to the measurement technique itself. Identifying these contributing sources of measurement uncertainty provides insight into ways of assessing and improving data quality. Established methods for uncertainty analysis have been developed and standardized.¹⁸ The focus of the present work is to apply these methods to rotor blade tip vortex LDV measurements using a procedure similar to that reported by Martin & Britcher in Ref. 19.

Past research into uncertainties in rotor wake measurement techniques has included studies of flow aperiodicity (vortex meandering) and flow seeding issues.^{20,21} Rotor wake scaling issues are outside the scope of the present paper, but future work is needed in this area. The current analysis is focused entirely on the measurement process in terms of optical calibration, data acquisition, and data reduction. The primary objective is to produce "uncertainty estimates based on professional calibrations of facilities and instrumentation, a thorough review of the process producing the data, and comprehensive accounting of significant biases inherent in the experiment."¹⁸

Experimental Apparatus and Procedures

A three-component LDV system was used in the present experiments. The rotor test stand and LDV configuration are shown in Figs. 1 and 2. This system separated a single multi-line Argon-Ion laser beam into three pairs of beams, each of which measured a single

component of velocity. A Bragg cell capable of frequency shifts of up to 40 MHz was used to produce the second shifted beam of each pair. Frequency shifts on each channel were optimized for the range of the bandpass filters. A rotary encoder enabled the data to be tagged with blade azimuth information with a resolution of 0.1° . Measurements were acquired within a time coincidence window ranging from 20 to $800\ \mu\text{s}$. This window ensured that all phase resolved measurements were statistically correlated on all three channels. Spatial coincidence of the three probe volumes was ensured to within a $25\ \mu\text{m}$ radius using an alignment technique to be described.

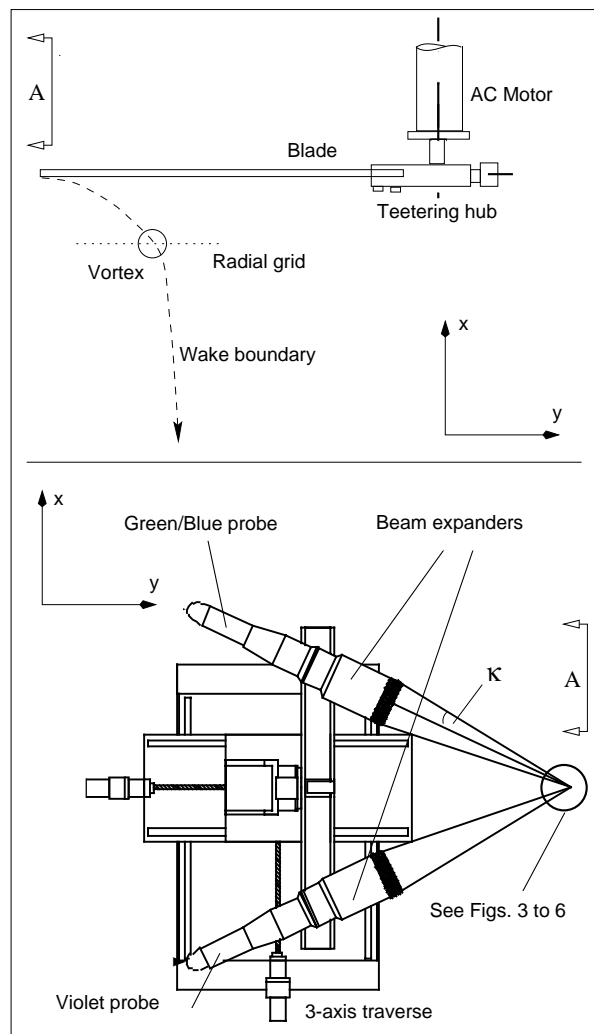


Figure 1: Rotor blade model, LDV optics, and traverse in the non-rotating hub fixed reference frame

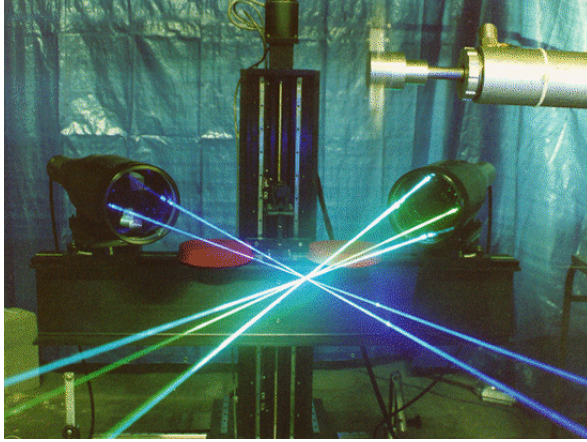
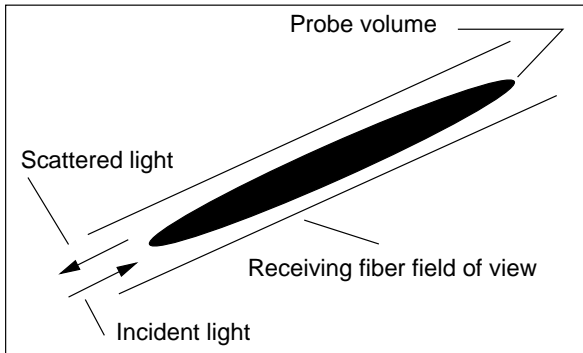


Figure 2: Hover test stand with 3-D LDV system

(a) On-axis backscatter light collection mode



(b) Off-axis backscatter light collection mode

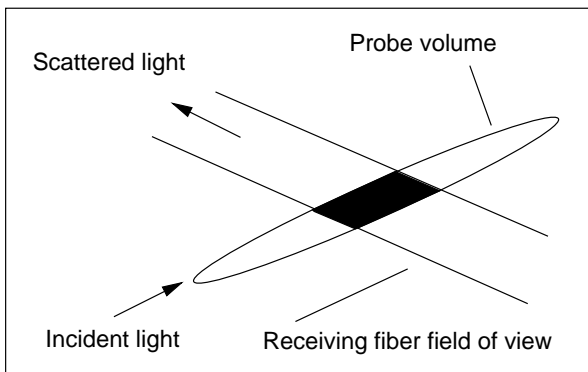


Figure 3: Schematic of receiving optics configuration

- (a) On-axis backscatter
- (b) Off-axis backscatter

Seed particles were generated using atomized olive oil passed through a spherical impactor. The resulting seed cloud was directed away from the flow field to prevent the ingestion of turbulence. The mean seed particle size was $0.6 \pm 0.2 \mu\text{m}$ in terms of aerodynamic

diameter, which has been shown to minimize the particle tracking errors in a vortical flow field.²⁰ The one-bladed rotor models were of 410 mm radius and balanced with a counterweight. Various tip shapes were studied at a nominally constant blade loading of $C_T/\sigma_e = 0.087$. The tip Mach number and Reynolds number of a rectangular baseline blade were 0.3 and 300,000 respectively.

LDV Optics Configuration

Scattered light from the particles was received in either the 'off-axis' or standard 'on-axis' configurations. These two configurations were used in an attempt to improve coincident data rates and to clarify the effect of spatial resolution on the measured vortex properties. In the on-axis configuration, scattered light is received in direct backscatter mode, as shown in Fig. 3a. As a result, the entire length of the probe volume is visible to the receiving optics. Note that the length of the probe volume can be more than ten times its width, especially when large standoff distances are required in wind tunnels, e.g. Refs. 1 and 5. The ratio of the probe volume width to length is approximately κ , the half-angle of the beam crossing in radians (see Fig. 1). One method of reducing the probe volume length is by increasing the crossing angle using the 2.6X beam expanders as shown in Figs. 1 and 2. Another method is to reduce the effective size of the probe volume visible to the receiving optics using an off-axis backscatter technique.²² The probe to the left in Fig. 2 transmits the violet beams, and the probe to the right is used to receive the scattered light from the violet probe volume. Similarly, the probe to the right in Fig. 2 transmits the blue and green beams, and the probe to the left is used to receive the scattered light. This spatially filters the scattered light, as shown in Fig. 3b.

While the scattered light intensity of the Mie pattern is much less at this collection angle, the signal-to-noise ratio is higher. Detectable bursts originating away from the center of the probe volume are effectively noise when coincidence is required for all three channels. Only the data from the center portion of each of the probe volumes is truly coincident in space. In the on-axis configuration, the receiving fiber views the entire probe volume length – most of which is producing bursts that are not occurring on the other two channels. The off-axis view of the receiving fiber spatially filters the regions of the probe volume generating measurable, but not coincident, bursts. For this reason, the overall signal-to-noise ratio is improved by requiring both spatial and temporal coincidence. Note that geometric coincidence determines the spatial resolution of the probe volume. Temporal coincidence

ensures that a characteristic flow structure convecting past the probe is statistically correlated on all channels.

LDV Beam Alignment Technique

In an effort to further reduce the uncertainty in the beam crossing angles while quantifying the spatial resolution, an alignment technique was developed and applied using a laser beam profiler. The three-dimensional geometry of all six intersecting beams shown in Fig. 2 was measured with a laser beam profiler. The field of view of the receiving optics was also measured by transmitting light from the receiving fiber to the probe volume. A similar apparatus was used by Miles & Witze³⁰ to quantify fringe spacing of a one component system. Another technique of alignment used a 25 μm pinhole aperture placed in front of a laser power meter.²² The pinhole technique was found to be effective but much more time consuming than using a profiler.

The profiling system used in the present work consists of a scanhead mounted on a tripod, and a data acquisition card connected to a personal computer. The main component of the scanhead is an entrance aperture that allows multiple beams to be targeted onto a rotating drum. On opposite sides of the rotating drum, two slits (1 μm wide) are orientated at ± 45° with respect to the rotation of the drum. As a result, one slit traverses the incident beams along a horizontal axis, while the other traverses along a vertical axis. Within the drum a large area silicon photodetector is used along with a load resistor to measure the beam irradiance profile as the slits scan through the beam.

The spatial resolution of the profile measurement was 0.14 μm and a typical standard deviation for a beam waist measurement was 0.25 μm (using 50 samples at 10 Hz). It is important to note that a single beam is profiled simultaneously in both axes in approximately 5 sec. This is one of the primary advantages over the pinhole alignment technique that requires the beam to be traversed independently across the pinhole in both axes. It is important to note that all six beams can be profiled in both axes of the 10 mm target area near the beam crossing without moving the scanhead or traverse. It is this large viewing area and high spatial resolution that have proven this technique to be a valuable tool for aligning multiple component LDV systems. Power limitations require that only one or two beams can be incident on the scanhead at a given time, but the location and profile of all six beams can be measured in a matter of minutes by turning individual beams on and off using shutters on the fiber optic couplers.

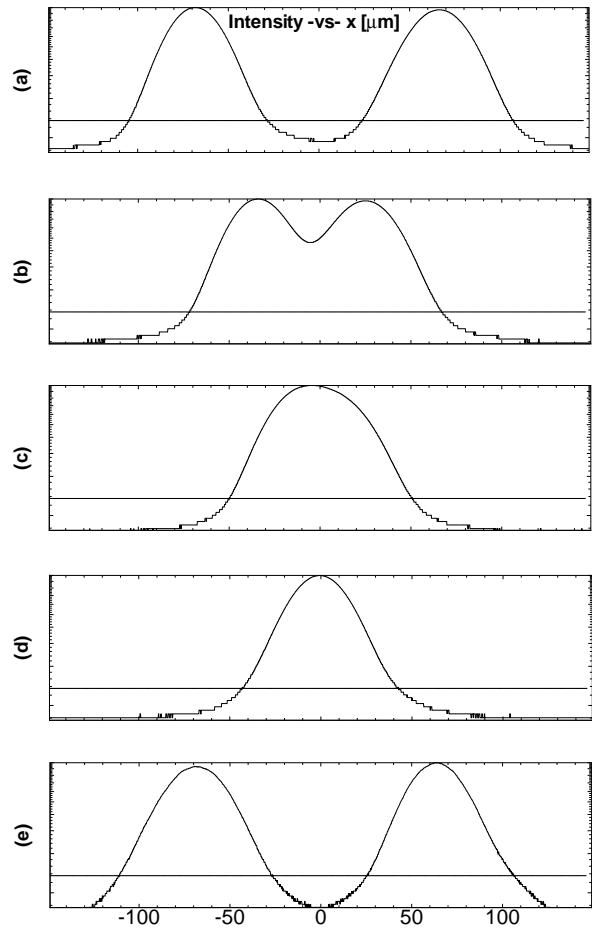
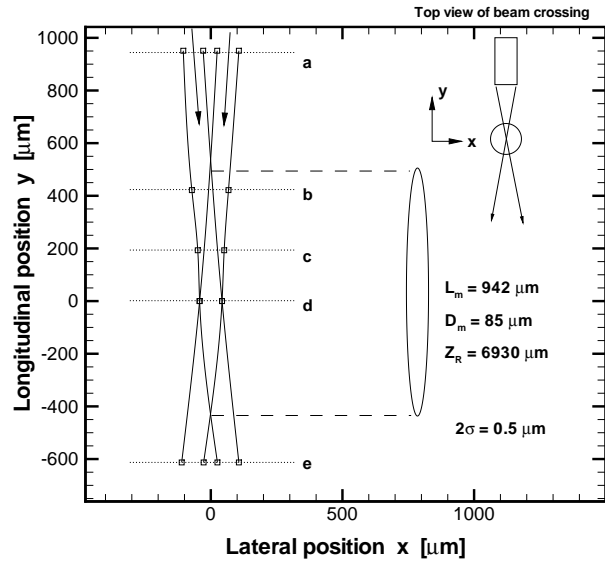


Figure 4: Laser beam profile measurements

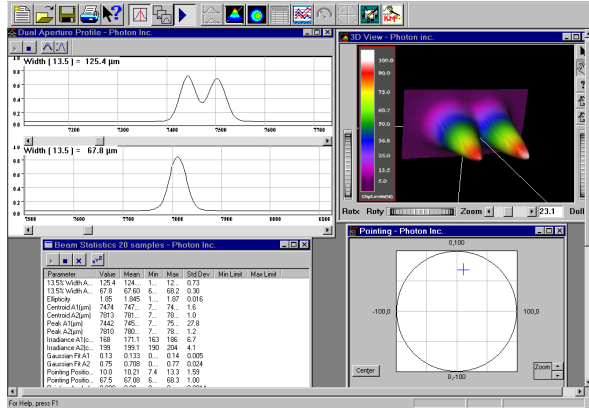


Figure 5: Screen shot of beam profiling at station (b)

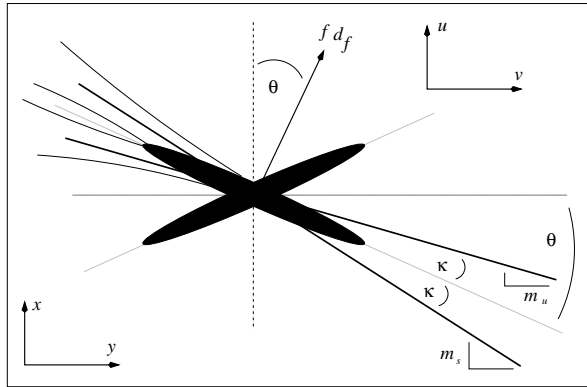


Figure 6: Example beam alignment of one channel

The alignment technique involves measuring the beam profiles in several planes by traversing the fiber optic probes. The alignment of the receiving fibers is also performed by transmitting light from the fiber to the measurement region. The centroid of the speckle spot intensity distribution was measured, as well as its width.

Example results of profiling one pair of beams are presented in Fig. 4. The intensity profile is shown at several stations (a-e) before, during, and after the beam crossing. The standard $1/e^2$ threshold was used to define the width of the beam in each axis, and the cutoff is shown as a dotted line in Fig 4. By profiling the beams both as a pair and individually, the beam crossing can be aligned with the beam waists. An example screen shot in Fig. 5 illustrates the real time view of the beam crossing. The targeting window was

found to be extremely useful in the alignment process. In addition, the Rayleigh length, Z_R , of each beam was measured. The Rayleigh length is a measure of the effective length of the beam waist and is approximately six times the length of the probe volume. The long effective waist of all six beams is one primary source of inaccurate alignment of multi-component LDV systems.

After alignment, the profiler technique also provided a more accurate method for measuring the half angle of the beam crossing. The half angle was measured by moving the fiber optic probes along the y -axis using the traverse and measuring the displacement of the beams in the x and z directions using the beam profiler - see Fig. 6. For each pair of beams, the slope of the shifted and unshifted beams is m_s and m_u , respectively. The slope

$$m = \frac{\Delta y}{\Delta x} \quad (1)$$

of each beam is used to determine the half angle of the beam crossing, κ , where

$$\kappa = \frac{\tan^{-1}(m_s) - \tan^{-1}(m_u)}{2} \quad (2)$$

and the fiber optic probe transmitting angle, θ , where

$$\theta = \frac{\pi}{2} - \frac{\tan^{-1}(m_s) + \tan^{-1}(m_u)}{2} \quad (3)$$

The profiler was capable of accepting beams within a 45° cone of acceptance with respect to its face.

Measurement Technique

This section begins with a general description of a phase-resolved velocity measurement. Next, the method is specialized for the case of measuring the velocity profile of a convecting vortex. The flow field velocity is measured at a position in the fixed hub frame of reference (x, y, z) as a function of the rotor blade azimuth, ψ . It is assumed that the mean velocity at a fixed point in space is a periodic function of ψ , i.e.,

$$V = V(x, y, z, \psi) \quad (4)$$

The probe volume is traversed along the y -axis across a radial grid fixed in space in the non-rotating hub frame of reference - see Fig. 1. The blade rotates at an angular rate, Ω , with respect to the fixed hub and grid.

At a specific blade position with respect to the grid, ψ , the phase-resolved velocity, u' , is measured. The phase-resolved velocity is an average over the phase resolution, res_ψ , sometimes called the "bin" width, i.e.,

Measurement Uncertainty Analysis

At a specific value of ψ , the phase-resolved velocity is reported as a mean value and an uncertainty at the 95% confidence level, i.e.,

$$V(x, y, z, \psi) = \bar{V} \pm \delta V \quad (95\%) \quad (10)$$

For clarity, the prime notation of the previous section has been dropped, and it is understood that the velocity in this section is the phase-resolved velocity. The objective of this section is to rigorously determine the measurement uncertainty δV in the velocity according to the established industry standards.¹⁸

The velocity, \bar{V} , is the product of a transformation matrix and a vector of Doppler frequencies, i.e.,

$$\bar{V}(x, y, z, \psi) = \begin{bmatrix} u \\ v \\ w \end{bmatrix} = [A][F] \quad (11)$$

The transformation matrix is based purely on the geometric configuration of the optics

$$[A] = \begin{bmatrix} d_{f_1} \frac{\sin \theta_3}{\sin(\theta_1 + \theta_3)} & 0 & d_{f_3} \frac{\sin \theta_1}{\sin(\theta_1 + \theta_3)} \\ d_{f_1} \frac{\cos \theta_3}{\sin(\theta_1 + \theta_3)} & 0 & d_{f_3} \frac{-\cos \theta_1}{\sin(\theta_1 + \theta_3)} \\ 0 & d_{f_2} & 0 \end{bmatrix} \quad (12)$$

where d_f is the fringe spacing and θ is the transmitting angle of each channel. Channels 1, 2, and 3 correspond to green, blue, and violet, respectively. Details of the optics configuration are given in Fig. 6. The Doppler frequency is the difference between the measured burst frequency, ν , and the shift frequency setting, s , for each channel, i.e.,

$$[F] = \begin{bmatrix} f_1 \\ f_2 \\ f_3 \end{bmatrix} = \begin{bmatrix} \nu_1 - s_1 \\ \nu_2 - s_2 \\ \nu_3 - s_3 \end{bmatrix} \quad (13)$$

Under the assumptions of the fringe model, LDV is based on a direct measurement of ν , the burst frequency of light scattered from seed particles passing through the fringe pattern of the probe volume. Following Ref. 31, the multiple measurement uncertainty analysis is divided into three steps:

(1) Calibration uncertainty. The study of sources of uncertainty in the alignment of the optics $\delta[A]$.

(2) Data acquisition uncertainty. The study of the sources of uncertainty in the frequency measurements $\delta[F]$.

(3) Data reduction uncertainty. The study of the propagation of the sources of uncertainty $\delta[A]$ and $\delta[F]$ to the final result.

For each source, the total uncertainty, δ , is a function³² of the source bias limit, B , the source precision limit, P , and a student t-factor, $t_{v,95}$, i.e.,

$$\delta = \sqrt{B^2 + (t_{v,95}P)^2} \quad (95\%) \quad (14)$$

The source limits are a combination of elemental types of bias and precision uncertainty²⁹

$$B = \sqrt{\sum_{i=1}^N B_i^2} \quad \text{and} \quad P = \sqrt{\sum_{i=1}^N P_i^2} \quad (15)$$

The student t-factor is found using Table 2-A-1 of Ref. 18. It is assumed that the sources of uncertainty are random and independent errors. This allows the sources to be combined in quadrature according to the Kline-McClintock second power law.³² For a generic function g , of N independent variables, x_i , we have

$$g = g(x_1, x_2, \dots, x_i, \dots, x_N) \quad (16)$$

and the uncertainty is given by

$$\delta g = \sqrt{\sum_{i=1}^N \left(\frac{\partial g}{\partial x_i} \right)^2 (\delta x_i)^2} \quad (17)$$

Calibration Uncertainty

The total uncertainty in the alignment of the optics, $\delta[A]$, can be decomposed into two primary source groups. The first group consists of elemental sources contributing to the uncertainty in the fringe spacing, d_f . The second group consists of elemental sources contributing to the uncertainty in the transmitting angle, θ .

The fringe spacing is determined by measuring the half angle of the beam crossing, κ , using

$$d_f = \frac{\lambda}{2 \sin \kappa} \quad (18)$$

where λ is the wavelength of the beams. The half angle and the transmitting angle were measured by the procedure described in the LDV beam alignment section using Eqs. 1-3. The uncertainty in the fringe spacing depends on the specific alignment technique. Using Eq. 17 and Eq. 18, the uncertainty in the fringe spacing is found to be

$$\frac{\delta d_f}{d_f} = \frac{2m \cos^2 \kappa}{(1+m^2)} \sqrt{\left(\frac{\delta x}{\Delta x} \right)^2 + \left(\frac{\delta y}{\Delta y} \right)^2} \quad (19)$$

Similarly, the uncertainty in the transmitting angle is

$$\delta\theta = \frac{m}{1+m^2} \sqrt{\left(\frac{\delta x}{\Delta x}\right)^2 + \left(\frac{\delta y}{\Delta y}\right)^2} \quad (20)$$

Typical values of the constants are

$$m = 2, \kappa = 5^\circ, \Delta x = 600 \mu m, \Delta y = 1200 \mu m$$

The next task is to estimate the uncertainty in δx and δy using Eqs. 14 and 15.

Sources of bias are neglected for both the beam profiler measurement of x and the traverse reading y . One source of precision uncertainty is the instrument resolution: $\text{res}_x = 0.14 \mu m$, $\text{res}_y = 5 \mu m$. For the beam profiler, an additional source is the standard deviation, $\sigma_x = 0.25 \mu m$ (sample size of $N_x = 50$, $t_{v,95} = 2$). The total uncertainty in the beam position measurement is given by

$$\delta x = 2 \sqrt{\left(\frac{\sigma_x}{\sqrt{N_x - 1}}\right)^2 + \left(\frac{\text{res}_x}{2}\right)^2} \quad (95\%) \quad (21)$$

$$\delta y = 2 \sqrt{\left(\frac{\text{res}_y}{2}\right)^2} \quad (95\%) \quad (22)$$

Substituting typical values of the constants provides the desired uncertainty estimate of the terms in Eq. 12, i.e.

$$\begin{aligned} \delta x/x &= \pm 0.03 \% & \delta y/y &= \pm 0.4 \% \\ \delta d_f/d_f &= \pm 0.3 \% & \delta\theta/\theta &= \pm 0.4 \% \end{aligned} \quad (23)$$

Obviously, the alignment method could be further improved by using an optical stage with a micrometer instead of the LDV traverse to reduce δy .

Data Acquisition Uncertainty

The objective of this section is to estimate the total uncertainty in the Doppler frequency, δf . This is approximated using Eq. 13 as

$$\frac{\delta f}{f} \approx \frac{\delta\nu}{\nu} \quad (24)$$

The uncertainty in the frequency shift setting is neglected based on the specifications for the Bragg cell. Using Eq. 14, the total uncertainty in the frequency measurement is

$$\delta\nu = \sqrt{B_\nu^2 + (t_{v,95} P_\nu)^2} \quad (25)$$

which is a combination of a source bias limit, B_ν , and a source precision limit, P_ν .

The source bias limit is based on several elements, namely

$$B_\nu = \sqrt{B_f^2 + B_V^2 + B_g^2 + B_a^2 + B_s^2 + B_w^2} \quad (26)$$

where the terms under the radical are defined as fringe bias, velocity bias, gradient bias, angle bias, seeding bias, and filter window bias, respectively. For a complex flow field such as a helicopter rotor wake, it is critically important to estimate and minimize the frequency source bias limit, B_ν . For this reason, each LDV bias source warrants its own discussion and will be presented later.

The remainder of this section estimates the source precision limit. The source precision limit, P_ν , is based on the phase resolution, res_ψ , the standard deviation of the frequency measurement, σ_ν , and the frequency resolution, res_ν , i.e.,

$$P_\nu = \sqrt{\left(\frac{\partial\nu}{\partial\psi} \frac{\text{res}_\psi}{2}\right)^2 + \left(\frac{\sigma_\nu^2}{N_\nu - 1}\right) + \left(\frac{\text{res}_\nu}{2}\right)^2} \quad (27)$$

The first term under the radical is unique to phase-resolved LDV measurements. At a point in space, the velocity varies periodically with the phase (ψ) of the rotor blade. The source of this uncertainty is that a finite resolution is used to discretize a continuous velocity signature - see Eq. 5. It is important to note that in practice, improving the phase resolution (decreasing res_ψ) tends to reduce the number of samples N_ν collected during a given sampling period. This is especially true in the case of a hovering rotor wake where flow seeding becomes difficult.²⁰ To minimize the source precision limit, preliminary measurements are required to understand the seeding issues and to estimate the frequency gradient $\partial\nu/\partial\psi$. Another reason is that the source precision limit is highly dependent on the critical flow features. For example, a vortex core convecting along the rotor wake boundary is characterized by a seed void (low N_ν), a substantial turbulence level (high σ_ν), and flow reversal (high $\partial\nu/\partial\psi$). Each of these contributions increase the source precision limit solely on the basis of the inherent flow physics.

The process of capturing a vortex on the LDV measurement grid was shown sequentially in Fig. 7 with example measurements in Figs. 8 and 9. This allows an estimate of the gradient $\partial\nu/\partial\psi$ to be made as a function of distance across the core - see the curve fit to the measurements shown in Fig. 10. The terms under the radical of Eq. 27 are plotted in Figs. 10 through 12. The frequency resolution of the autocorrelation based digital burst correlator is $\text{res}_\nu/\nu = 0.05\%$. Figure 12 shows the final result of the distribution of the precision term of Eq. 25 across the vortex core for a single LDV channel.

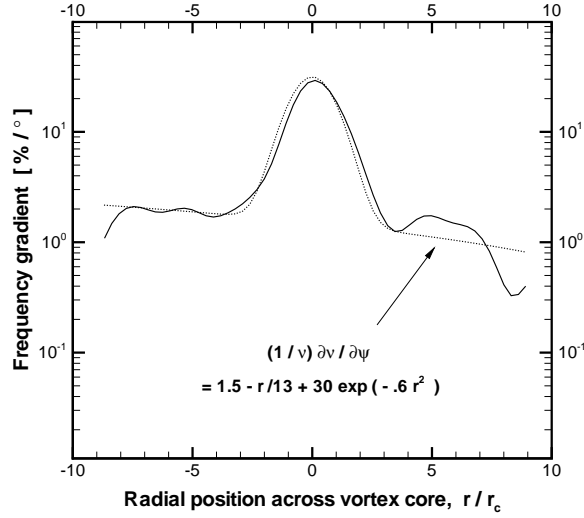


Figure 10: Frequency gradient across vortex core

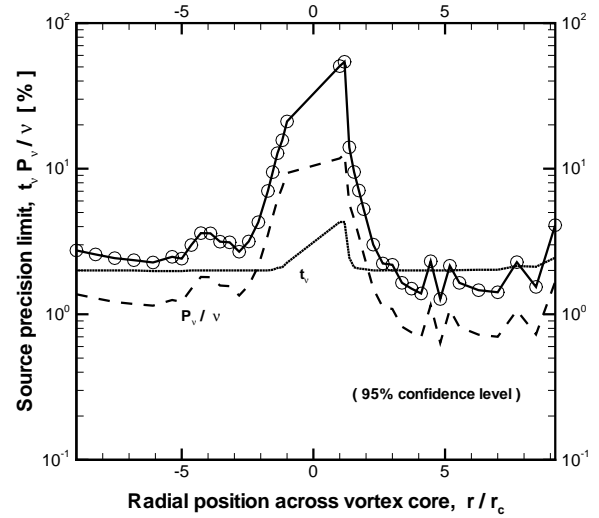


Figure 12: Frequency source precision limit across vortex core

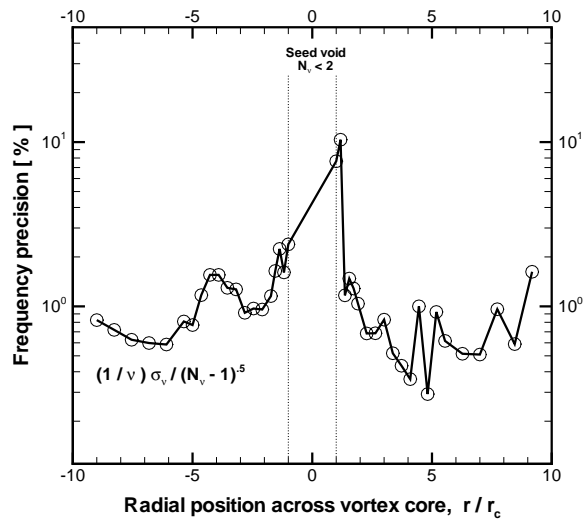
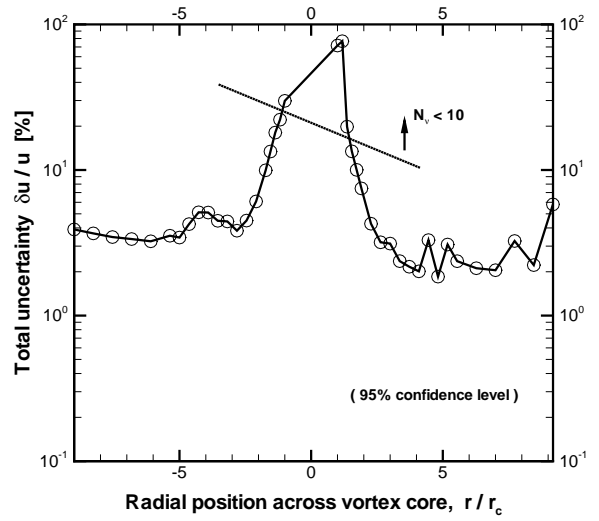


Figure 11: Frequency precision across vortex core


 Figure 13: Total measurement uncertainty $\delta u/u$ across vortex

Data Reduction Uncertainty

Having presented the fundamental sources of uncertainty, $\delta \bar{A}$ and $\delta \bar{F}$, this section presents the results of how these sources combine to add to the final uncertainty in velocity, i.e.,

$$\delta \bar{V} = \sqrt{\delta \bar{A}^2 + \delta \bar{F}^2} \quad (28)$$

It is assumed that for the uncertainty estimate $\theta_1 \approx \theta_3$. It is also assumed that the relative errors in fringe spacing and frequency are the same for all channels. The total measurement uncertainty in the three components of velocity is

$$\frac{\delta u}{u} = \sqrt{2 \tan^2 \theta \delta \theta^2 + 2 \left(\frac{\delta d_f}{d_f} \right)^2 + 2 \left(\frac{\delta f}{f} \right)^2}$$

$$\frac{\delta v}{v} = \sqrt{2 \cot^2 \theta \delta \theta^2 + 2 \left(\frac{\delta d_f}{d_f} \right)^2 + 2 \left(\frac{\delta f}{f} \right)^2} \quad (29)$$

$$\frac{\delta w}{w} = \sqrt{\left(\frac{\delta d_f}{d_f} \right)^2 + \left(\frac{\delta f}{f} \right)^2}$$

An example of the uncertainty distribution across the vortex core is shown in Figure 13. The uncertainty

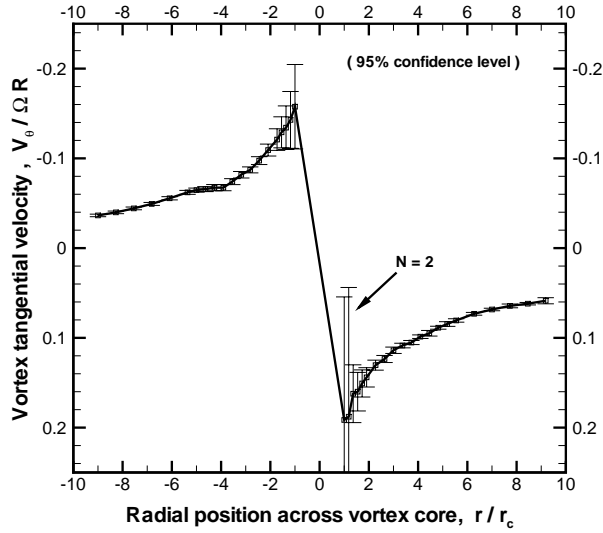


Figure 14: Vortex tangential velocity profile with error bars

increases dramatically near the core boundary as a result of the small sample size associated with the seed void and the increased standard deviation associated with viscous core turbulence. This represents an important step in estimating the magnitude and cause of vortex measurement uncertainty. Using this result, future tests must be focused on developing methods of improving data quality near the core boundary.

For the hover test case of this configuration, the nondimensional peak swirl velocity is

$$V_{\theta} = -\frac{u'}{\Omega R} \quad (30)$$

and so the measurement uncertainty is

$$\frac{\delta V_{\theta}}{V_{\theta}} = \sqrt{\left(\frac{\delta u}{u}\right)^2 + \left(\frac{\delta \Omega}{\Omega}\right)^2 + \left(\frac{\delta R}{R}\right)^2} \quad (31)$$

A representative vortex profile with uncertainty bars shown in Fig. 14 illustrates why reporting a single number for uncertainty can be misleading. This is especially true when the peak swirl velocity is used for CFD validation.

Sources of LDV Frequency Bias

When discrepancies occur between rotor vortex measurements acquired at different facilities, one of the most popular explanations is differences in flow aperiodicity.^{13,21} For this reason, a honeycomb/screen flow conditioning cell was constructed around the current test stand, and aperiodicity levels have been quantified and analyzed.²¹ Other researchers have also gone to great lengths to reduce flow aperiodicity. Even

so, discrepancies exist in the most fundamental physical observations of vortex core properties measured using LDV at similar flow scales.

The current results indicate another possible explanation is measurement accuracy. While it is fairly certain that the precision of measurements (if reported) should not be expected to vary between facilities, the same conclusion cannot be drawn for measurement accuracy. The reported uncertainty in LDV measurements must include a quantitative estimate and discussion of sources of frequency bias found in Eq. 26. A complete discussion of filter window bias, B_w , and angle bias, B_a , is presented in Ref. 38. The remaining sources of bias will be treated in the following sections.

Fringe Bias

The source of this form of bias is a nonuniformity in fringe spacing caused by optical misalignment. A theoretical indicator of the uniformity of fringe spacing in the measurement volume has been given by Zhang & Eisle³³ in terms of a fringe distortion number. Fringe distortion is proportional to the distance between the point of beam crossing and the beam waist. Maximum fringe visibility and uniformity occur when the beams are aligned to cross at their waists. Using the beam profiler alignment technique described previously, this parameter can now be both quantified and minimized to negligible values.

Seed Particle Bias

The source of this form of bias is a difference between the velocity of the fluid and the velocity of the seed particles. The seed particle dynamics and associated velocity error is covered in detail in Ref. 20. The same method is extended for a quasi-steady analysis of a diffusing vortex using LDV velocity field measurements as an input to a particle dynamics analysis. The relationship between the seed void and the vortex core size can be estimated as a function of wake-age for a range of particle size, which is shown in Fig. 15. Current research is focused on developing an empirical technique of acquiring the same information. Even though the particle size is usually chosen to minimize this form of bias, a discrepancy between the seed void and core size can still occur as a small velocity error is integrated over time.

Velocity Bias

The source of this form of bias is the dependency of the rate of seed particles traveling through the probe volume on the flow velocity. The result is a nonuniform sampling of the distribution of velocity about a mean value. Higher velocity particles are sampled more often

than low velocity particles, and so the mean value of the distribution becomes biased. This source of bias is increased by the level of turbulence and can become severe when the measurement also suffers from poor spatial resolution.

For phase resolved LDV a velocity bias correction is applied on a bin-by-bin basis using transit time weighting. The mean velocity at a given point in space and at a fixed blade azimuth is a weighted mean using

$$\bar{V} = \frac{\sum_{i=1}^N V_i \tau_i}{\sum_{i=1}^N \tau_i} \quad (32)$$

which is based on the transit time of the seed particle. Even though a bias correction is applied, the uncertainty still exists and can be estimated using

$$B_V = \sqrt{\left(\bar{V} - \frac{1}{N} \sum_{i=1}^N V_i \right)^2} \quad (33)$$

Figure 16 shows the estimated uncertainty measured across a representative vortex core at a wake-age of $\zeta = 75^\circ$.

Velocity Gradient Bias

The presence of a velocity gradient across a finite length probe volume is the source of this form of bias. In the previous section, velocity bias assumes an infinitely small probe volume and involves the temporal variation of velocity at a fixed point in space. In this section, velocity gradient bias considers the effect of a finite probe volume in the presence of a spatial variation of velocity at a fixed time. This section of the paper is expanded in detail based on the recommendation of Edwards.³⁸

Historically, gradient bias has been one of the fundamental problems in the measurement of shear layers using a variety of instruments including Pitot tubes, hotwires, and LDV.²⁷ The error in the measured mean velocity is a function of the spatial resolution of the instrument compared to the scale of the shear layer. Furthermore, the error is proportional to the velocity gradient and can be expressed in terms of

$$\alpha = \frac{L_m}{L} \frac{\partial(u/U_o)}{\partial(y/L)} \approx \frac{L_m}{L} \quad (34)$$

where L_m is the spatial resolution, and L is the length scale of the shear layer.

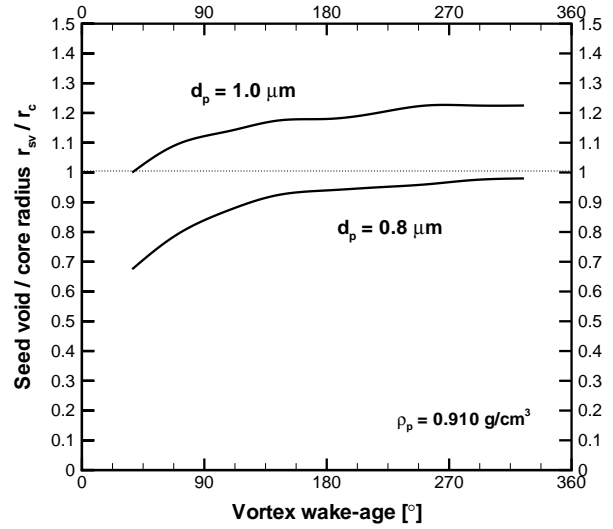


Figure 15: Ratio of seed void to core radius as a function of wake-age

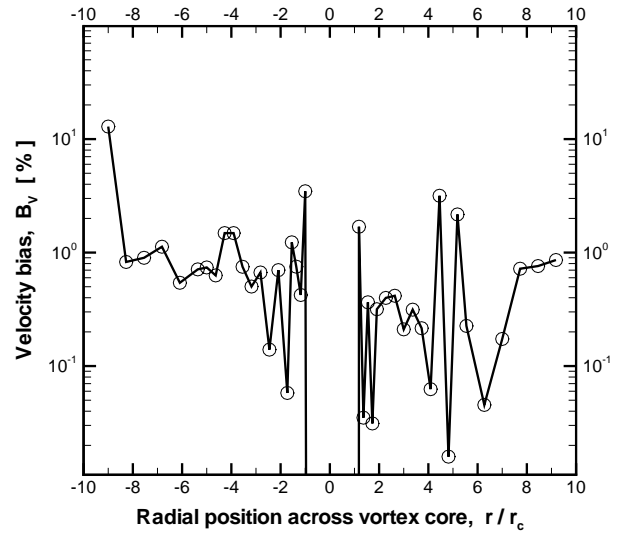


Figure 16: Measured velocity bias across vortex core

The frequency bias associated with LDV spatial resolution was theoretically investigated in Ref. 37. For a given shear layer, the uncertainty grows with the square of the spatial resolution, that is

$$B_g \propto \alpha^2 \quad (35)$$

Applying the theoretical method³⁷ to a 2D self-similar vortex flow field, gradient bias was estimated for varying ratios of probe volume length to core radius. The predicted error in the peak swirl velocity is plotted as a function of L_m/r_c in Fig. 17. Note that a probe volume length of $0.1r_c$ is required to reduce the error to

less than 0.1% over the entire velocity profile. Considering a representative case of a viscous vortex core with a dimensional radius of approximately 2 mm (at model scale), the probe volume length is limited in theory to 200 μm . This is much less than the standard length measured by the beam profiler in Fig. 4. This is why an off-axis alignment of the receiving optics should generally be used to spatially filter the visible length of the probe volume.

Figure 18 shows the theoretical results for an example vortex profile. The asymmetry in the error is confirmed by the results of Ref. 37, which states that the net error depends on the relative magnitudes of the first and second derivatives of the velocity profile. As shown by Figs. 17 and 18, considerable error may be introduced when the probe volume length is of the order of the vortex core radius. Extending the analysis to the case where a vortex velocity profile is primarily measured by two channels, the net error increases by a factor of 1.4 over the single component result. For this reason a spatial resolution of $\leq 0.05r_c$ is recommended, and a value of $0.03r_c$ is used for the present experiments. Note that unsteady effects, such as turbulence, tend to increase this form of velocity error.³⁷

In support of these theoretical results, an experiment was conducted on a rotor tip vortex for two different ratios of probe volume length to core radius, L_m/r_c . In the standard on-axis configuration with a large coincidence window (1 sec), the ratio was $L_m/r_c = 0.3$ compared to the ratio of $L_m/r_c = 0.03$ for the off-axis configuration. The results measured across the vortex for both cases are compared in Fig. 19. The significant effect of the optics configuration on the velocity profile was measured to be repeatable for a given vortex. All test conditions were held constant except for the angle of the scattered light collection.

It was noted that the signal-to-noise ratio also played a role in the velocity error. This could be one reason why the theoretical results underestimate the apparent magnitude of the measured gradient bias. The reduced noise of an off-axis configuration in a 3D boundary layer has been noted by Ref. 36. In another boundary layer study, the length of the measurement volume was effectively reduced by receiving light in a side scatter configuration using a pinhole as a spatial filter to reduce noise.³⁵

Using preliminary LDV measurements and a flow visualization technique,³⁹ the vortex convection velocity can be estimated in both the radial and axial directions. Resolving the velocity field with respect to a coordinate system fixed to the vortex core, the phase-resolved data can be qualitatively mapped into a planar image of the

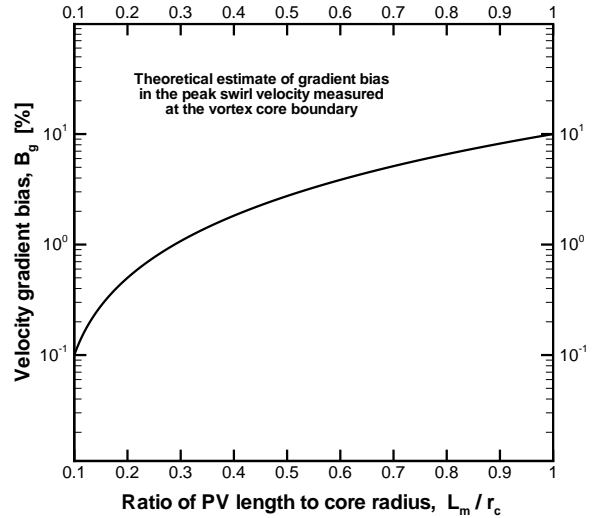


Figure 17: Spatial resolution error in vortex measurements

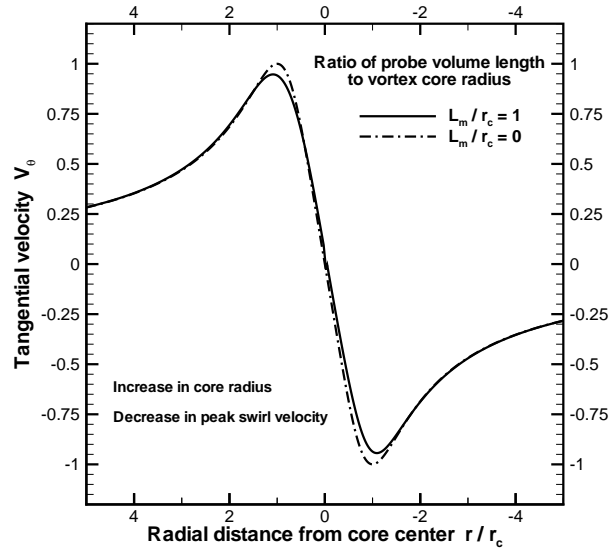


Figure 18: Theoretical effect of velocity gradient bias

vortex velocity field.⁵ The results shown in Fig. 20 are the streamlines computed from the measured velocity field at $\zeta = 75^\circ$. An example flow visualization image at the same wake-age is shown for comparison. The results show the distortion of the vortex core and sheet that occurs when gradient bias is substantial. This agrees with the results shown for a fixed wing vortex in Ref. 22.

To make accurate measurements of a wing or rotor blade tip vortex, it has been shown above that the spatial resolution of the measurement technique must be able to resolve the steep velocity gradients surrounding the core. In the case of fixed wing measurements, it is standard practice to quote the spatial resolution

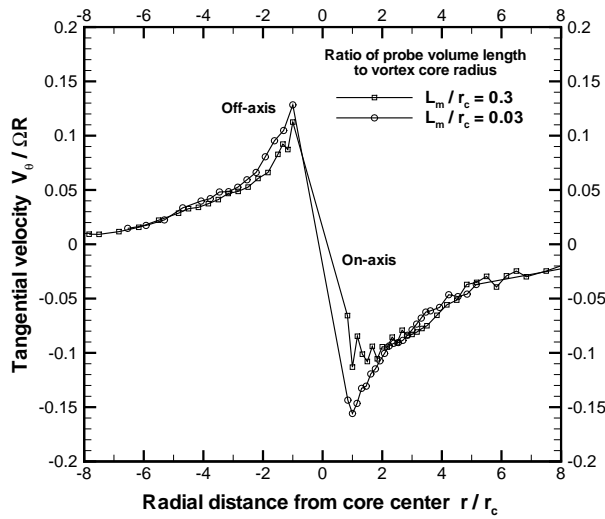


Figure 19: Measured effect of velocity gradient bias

of the technique. For comparison, the spatial resolution will be presented as the ratio of the probe size to the vortex core radius, $\alpha = L_m/r_c$. Typical fixed wing vortex measurements report a spatial resolution in the range $\alpha = 0.05$ to 0.2 using multi-hole pressure probes.²³⁻²⁶ The associated error was estimated to be minimized to 1% using a resolution of $\alpha = 0.1$ with a seven-hole probe. A similar requirement was found for resolving airfoil wakes using Pitot probes.²⁷⁻²⁸ According to Ref. 22, the spatial resolution of a 3-component LDV system should be near $\alpha \approx 0.05$ for both fixed-wing and rotor blade vortex measurements. This agrees with the current observations and results.

Table 1 gives a list of several rotor tests conducted over the past three decades in both hover and forward flight using either LDV or hotwire probes. When reported, the core radius is taken as the smallest measured value; otherwise, a value of 5% chord is used. For LDV, the probe size, L_m , is quoted as the probe volume length visible to the receiving optics. This is done to give an estimate of the magnitude of gradient bias. For hotwires, the probe size is quoted as the width of the probe support (i.e., distance between support prongs) to estimate the overall intrusiveness of the technique. The number of components is listed along with whether or not temporal coincidence was required during data acquisition to validate multi-component measurements.

Comparing data from different scales and flight conditions is difficult; however, general trends in the basic flow physics should agree. In either case, it is assumed that large discrepancies might occur when

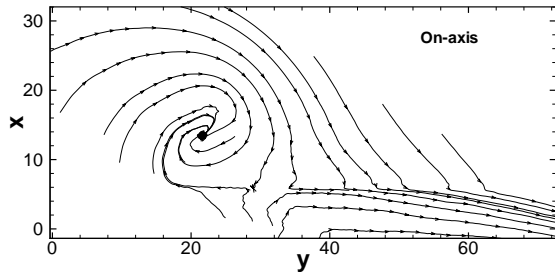
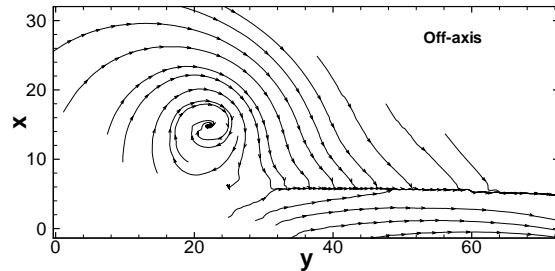
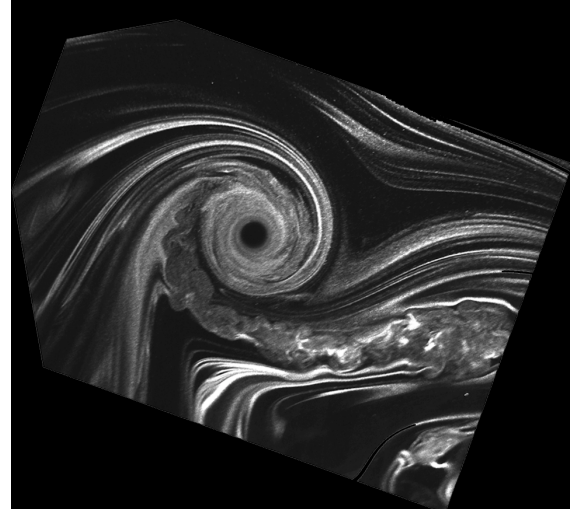


Figure 20 : Streamlines computed from LDV measurements
Off-axis $\alpha \approx 3\%$
On-axis $\alpha \approx 30\%$

comparing data between two tests when a significant difference in α exists. This hypothesis is confirmed in hover where the tip vortex core size was measured to increase⁶⁻⁸ with wake-age for $\alpha = 3\%$, and decrease¹³ with wake-age for $\alpha = 110\%$.

Conclusions

A precise LDV alignment technique utilizing a beam profiler to minimize measurement uncertainties was developed and described, including example results. The uncertainty in fringe spacing using this alignment technique is less than 0.5%. An uncertainty

Ref.	Author	Year	State	Description	Type	Method	Temporal Coincidence	L_m [mm]	r_c [mm]	0.05c [mm]	α [%]
5	Boutier	96	fflt	DNW HART	3D	LDV	Yes	.4	30	6	1
26	Devenport	99	fwng	VaTech	3D	HW	Yes	0.13	8	10	1.5
6-8	Leishman	95-00	hvr	Maryland	3D	LDV	Yes	0.08	3	2.2	3
22	Barrett	98	fwng	U. Bristol	3D	LDV	No	0.05	1	-	5
10	McAlister	95	hvr	Ames HTC	3D	LDV	No	0.5	10	9.6	5
4	Biggers	74-77	fflt	Ames 7x10	2D	LDV	No	1	7.5	5	17
11	Raffel	98	fflt	ILR Aachen	3D	LDV	Yes	1	4	2.7	25
12	Thompson	88	hvr	GaTech	1D	LDV	No	2	7.6	6.4	26
9	Mahalingam	98	fflt	GaTech	1D	LDV	No	2	7	4.4	29
15	Caradonna	81	hvr	Ames AHC	1D	HW	Yes	3	-	9.6	31
16	Cook	73	hvr	Westland	1D	HW	Yes	1.6	2.5	20	64
14	Tung	81	hvr	Ames AHC	1D	HW	Yes	3	-	3.8	79
17	Boatwright	72-74	hvr	Miss. St.	3D	HW	Yes	8	10	12	80
13	Wadcock	97	hvr	Ames OARF	1D	HW	Yes	3	2.7	2.8	110
1	Gorton	95	fflt	Langley 14x22	2D	LDV	No	5	3.3	2.1	150

Table 1: Summary of probe size versus vortex core size: fflt = forward flight, hvr = hover, fwng = fixed wing, LDV: L_m = probe volume length, HW : L_m = hotwire probe support width

analysis for phase resolved 3D LDV measurements of a rotor blade vortex core was derived in detail. The analysis used representative measurements at 75° wake-age. The procedure can be used as a framework for application to future tests. The following conclusions can be drawn from this study:

(1) It was shown that for phase-resolved 3D LDV measurements, the reported uncertainty estimates should include the distribution of precision and bias limits across the vortex core.

(2) The inherent physics of the flow increase the source precision limit near the vortex core boundary by several mechanisms. These include a reduction in sample size because of the seed void, an increase in standard deviation caused by core turbulence, and flow reversal associated with vortex convection.

(3) A quantitative estimate and discussion of sources of LDV measurement bias, especially gradient bias, should be included in vortex profiling experiments. The detrimental effects of gradient bias included reduction of the vortex peak swirl velocity and enlargement of the vortex core size.

(4) The spatial resolution of a 3D LDV system was shown to be an extremely important parameter, which should be defined in terms of the ratio α – the effective length of the probe volume to the smallest expected vortex core radius. Based on both theory and measurements, it is suggested that $\alpha \leq 5\%$ in vortical flows to minimize gradient bias.

(5) Operating in an off-axis backscatter light collection mode minimized α by spatially filtering the effective length of the probe volume.

Acknowledgments

This work was supported by the National Rotorcraft Technology Center under grant NCC 2944.

References

- [1] Althoff, S. G., Poling, D. R., and Dadone, L., "Laser Velocimetry and Blade Pressure Measurements of a Blade-Vortex Interaction," *Journal of the American Helicopter Society*, Vol. 40, pp. 15-23, 1995.
- [2] Berenger, T., Favier, D., Maresca, C., and Berton, E., "Experimental and Numerical Investigation of Rotor Aerodynamics in Forward Flight," 34th Aerospace Sciences Meeting, Reno, NV, AIAA 96-0676, 1996.
- [3] Biggers, J. C., Lee, A., Orloff, K., and Lemmer, O., "Measurements of Helicopter Rotor Tip Vortices," 33rd Forum, American Helicopter Society, Washington, D.C., pp. 1-11, 1977.
- [4] Biggers, J. C., and Orloff, K. L., "Laser Velocimeter Measurements of the Helicopter Rotor-Induced Flow Field," 30th Forum, American Helicopter Society, Washington, D. C., pp. 1-10, 1974.
- [5] Boutier, A., Lefevre, J., and Micheli, F., "Analysis of Helicopter Blade Vortex Structure by Laser Velocimetry," *Experiments in Fluids*, Vol. 21, pp. 33-42, 1996.
- [6] Han, O. Y., Leishman, J. G., and Coyne, A. J., "Measurements of the Velocity and Turbulent Structure of a Rotor Tip Vortex," *AIAA Journal*, Vol. 35, No. 3, pp. 477-485, 1997.
- [7] Leishman, J. G., Baker, A., and Coyne, A., "Measurements of Rotor Tip Vortices Using Three-Component Laser Doppler Velocimetry," *Journal*

- of the American Helicopter Society, Vol. 41, No. 4, pp. 342-353, 1996.
- [8] Martin, P. B., Leishman, J. G., Anderson, S., and Pugliese, G. J., "LDV and Stereoscopic PIV Measurements of the Vortex Wake of a Tapered Tip Rotor Blade," 56th Forum of the American Helicopter Society, Virginia Beach, VA, May, 2000.
- [9] Mahalingam, R., and Komerath, N. M., "Measurements of the Near Wake of a Rotor in Forward Flight," 36th Aerospace Sciences Meeting, Reno, NV, AIAA 98-0692, 1998.
- [10] McAlister, K. W., Schuler, C. A., Branum, L., and Wu, J. C., "3-D Wake Measurements Near a Hovering Rotor for Determining Profile and Induced Drag," NASA TP-3577, Aug. 1995.
- [11] Raffel, M., Seelhorst, U., and Willert, C., "Vortical Flow Structures at a Helicopter Rotor Model Measured by LDV and PIV," *The Aeronautical Journal*, April, pp. 221-227, 1998.
- [12] Thompson, T. L., Komerath, N. M., and Gray, R. B., "Visualization and Measurement of the Tip Vortex Core of a Rotor Blade in Hover," *Journal of Aircraft*, Vol. 25, No. 12, pp. 1113-1121, 1988.
- [13] Wadcock, A. J., "Measurement of Vortex Strength and Core Diameter in the Wake of a Hovering Rotor," AHS Technical Specialists' Meeting for Rotorcraft Acoustics and Aerodynamics, Williamsburg, VA, 1997.
- [14] Tung, C., Pucci, S. L., Caradonna, F. X., and Morse, H. A., "The Structure of Trailing Vortices Generated by Model Rotor Blades," NASA TM-81316, USAAVRADCOR TR-81-A-25, 1981.
- [15] Caradonna, F. X., and Tung, C., "Experimental and Analytical Studies of a Model Helicopter Rotor in Hover," *Vertica*, Vol. 5, pp. 149-161, 1981.
- [16] Cook, C. V., "The Structure of the Rotor Blade Tip Vortex," AGARD CP-111, pp. 3-1, 3-14, 1973.
- [17] Boatwright, D. W., "Measurements of Velocity Components in the Wake of a Full-Scale Helicopter Rotor in Hover," USAAMRDL Technical Report 72-33, 1972.
- [18] AIAA Standard, "Assessment of Wind Tunnel Data Uncertainty," AIAA S-071-1995.
- [19] Martin, P. B., Britcher, C. P., "Preliminary Flow Survey Measurements and Uncertainty Analysis from the Langley Full-Scale Wind Tunnel," AIAA 97-0010, 1997.
- [20] Leishman, J. G., "Seed Particle Dynamics in Tip Vortex Flows," *Journal of Aircraft*, Vol. 33, No. 4, pp. 823-825, 1996.
- [21] Leishman, J. G., "Measurements of the Aperiodic Wake of a Hovering Rotor," *Experiments in Fluids*, Vol. 25, pp. 352-361, 1998.
- [22] Barrett, R. V., and Swales, C., "Realisation of the Full Potential of the Laser Doppler Anemometer in the Analysis of Complex Flows," *The Aeronautical Journal*, June/July, pp. 313-320, 1998.
- [23] Bandyopadhyay, P. R., Ash, R. L., and Stead, D. J., "Organized Nature of a Turbulent Trailing Vortex," *AIAA Journal*, Vol. 29, No. 10, pp. 1627-1633, 1991.
- [24] Ash, R. L., and Stead, D. J., "Influence of Free Stream Turbulence on a Trailing Line Vortex," 3rd International Congress of Fluid Mechanics, Cairo, Egypt, pp. 345-358, 1990.
- [25] Chow, J. S., Zilliac, G. G., and Bradshaw, P., "Mean and Turbulence Measurements in the Near Field of a Wingtip Vortex," *AIAA Journal*, Vol. 35, No. 10, pp. 1561-1568, 1997.
- [26] Devenport, W. J., Vogel, C. M., and Zsoldos, J. S., "Flow Structure Produced by the Interaction and Merger of a Pair of Co-rotating Wing-tip Vortices," *Journal of Fluid Mechanics*, Vol. 394, pp. 357-377, 1999.
- [27] Chue, S. H., "Pressure Probes for Fluid Measurement," *Prog. Aerospace Sciences*, Vol. 16, No. 2, pp. 147-223, 1975.
- [28] Davies, P., "The Behaviour of a Pitot Tube in Transverse Shear," *Journal of Fluid Mechanics*, Vol. 3, pp. 441-456, 1958.
- [29] Abernathy, R. B., Benedict, R. P., and Dowdell, R. B., "ASME Measurement Uncertainty," *Journal of Fluids Engineering*, Vol. 107, pp. 161-164, 1985.
- [30] Miles, P. C., and Witze, P. O., "Fringe Field Quantification in an LDV Probe Volume by Use of a Magnified Image," *Experiments in Fluids*, Vol. 16, pp. 330-335, 1994.
- [31] Dunn, P. F., "Techniques of Measurement and Data Analysis," Technical Notes, University of Notre Dame, 1992.
- [32] Figliola, R. S., and Beasley, D. E., *Theory and Design for Mechanical Measurements*, John Wiley & Sons, Inc., Chap 5, 1991.
- [33] Zhang, Z., and Eisele, K., "On the Overestimation of the Flow Turbulence Due to Fringe Distortion in LDA Measurement Volumes," *Experiments in Fluids*, Vol. 25, pp. 371-374, 1998.
- [34] Zhang, Z., Eisele, K., and Hirt, F., "The Influence of Phase-Averaging Window Size on the Determination of Turbulence Quantities in Unsteady Turbulent Flows," *Experiments in Fluids*, Vol. 22, pp. 265-267, 1997.
- [35] Benedict, L. H., and Gould, R. D., "Understanding Biases in the Near-field Region of LDA Two-point Correlation Measurements," *Experiments in Fluids*, Vol. 26, pp. 381-388, 1999.
- [36] Compton, D. A., and Eaton, J. K., "A High-resolution Laser Doppler Anemometer for Three-dimensional Turbulent Boundary Layers," *Experiments in Fluids*, Vol. 22, pp. 111-117, 1996.
- [37] Kreid, D. K., "Laser-Doppler Velocimeter Measurements in Nonuniform Flow: Error Estimates," *Applied Optics*, Vol. 13, No. 8, pp. 1872-1881, 1974.
- [38] Edwards, R. V., "Report of the Special Panel on Statistical Particle Bias Problems in Laser Anemometry," *Journal of Fluids Engineering*, Vol. 109, pp. 89-93, 1987.
- [39] Martin, P. B., Bhagwat, M. J., Leishman, J. G., "Visualization of a Helicopter Rotor Wake in Hover," AIAA CP 99-3225, 1999.